Contribution from the Istituto per lo Studio della Stereochimica ed Energetica dei Composti di Coordinazione, CNR, Via J. Nardi 39, 50132 Firenze, Italy, Dipartimento di Chimica dell'Università di Siena, 53100 Siena, Italy, and Dipartimento di Chimica dell'Università di Firenze, 50100 Firenze, Italy

Homo- and Heterobimetallic Trihydride Complexes Stabilized by the Tripodal Phosphine Ligand $MeC(CH_2PPh_2)_3$: Experimental and Theoretical Studies

Claudio Bianchini,*[†] Franco Laschi,[‡] Dante Masi,[†] Carlo Mealli,*[†] Andrea Meli,[†] Francesca M. Ottaviani,[§] Davide M. Proserpio,[†] Michal Sabat,[∥] and Piero Zanello*[‡]

Received January 27, 1989

The trihydride (triphos)RhH_3 [triphos = $MeC(CH_2PPh_2)_3$] reacts with coordinatively unsaturated metal fragments to form a family of bimetallic polyhydride complexes of general formula $[(triphos)Rh(\mu\text{-}H)_3M(L)]^{n+}$ [M = Rh, Co, L = triphos, n = 3, 2, 1; M = Ni, L = triphos, n = 2, 1; M = Fe, L = $MeC(CH_2PEt_2)_3$, n = 2]. All of the compounds were isolated as BPh_4^-, ClO_4^-, or BF_4^- crystalline salts and their spectroscopic properties studied in detail by IR, NMR, and ESR techniques. The crystal structure of the paramagnetic homonuclear derivative $[(triphos)Rh(\mu\text{-}H)_3Rh(triphos)](BPh_4)_2$·DMF was established by X-ray methods. Crystal data: triclinic, $P\bar{1}$, a = 16.868 (4) Å, b = 15.863 (4) Å, c = 14.026 (3) Å, α = 111.74 (2)°, β = 91.01 (2)°, γ = 116.25 (2)°, Z = 1. The structure was refined to an R factor of 0.059 (R_w = 0.064) by using 9149 unique reflections with $I > 3\sigma(I)$. The complex cation consists of two pyramidal L_3Rh fragments (L = phosphine) held together by three bridging hydride ligands. The relative orientation of the L_3Rh fragments is halfway between eclipsed and staggered, the overall symmetry of the molecule being approximately D_3. The Rh-Rh separation measures 2.644 (1) Å. The electrochemical behavior in nonaqueous solvents shows that all of the compounds reversibly undergo multisequential one-electron-redox exchanges with no major variation of the primary geometry. NMR and ESR spectroscopies provide useful information concerning the geometric and electronic nature of diamagnetic and paramagnetic compounds, respectively. EHMO studies, not novel for this class of compounds, allow a new interpretation of the metal-metal bond in the dimers. In particular, the bond cannot be as strong as that predicted by simple electron-counting rules. Other comments are devoted to the potential existence of dimers with a bridging polyhydrogen unit [i.e. $\mu\text{-}H_3$ vs $(\mu\text{-}H)_3$]. Finally, the MO picture is used, on a very qualitative scale, to correlate structural, electrochemical, and spectroscopic parameters, in particular those derived from the ESR spectra.

Introduction

A perusal of the large body of experimental and theoretical information on polynuclear polyhydrides reveals the paucity of data on two particular classes of compounds, namely those that are built up by different metals and those that contain formally odd-electron metal centers.[1]

Distinctive features of heteronuclear polyhydrides appear to include their potential to give rise to more selective and efficient hydrogen-transfer reactions as well as to serve as models for the determination of hydrogen migration preferences on alloy phases.[2] In addition, given the reduced time scale of EPR vs NMR spectroscopy, paramagnetic polyhydrides are expected to be extremely useful in elucidating hydride mobility patterns over metal complexes (for example, bridged-terminal-hydride interconversion).[3] Furthermore, it is evident that hydrogen-transfer reactions directly accomplished by hydrides disregarding the 16- and 18-electron rule might serve to gain further insight into those hydrogenation reactions for which odd-electron pathways have been proposed.[4]

In this paper, we present how diamagnetic and paramagnetic, homo- and heterobimetallic transition-metal complexes containing bridging hydride ligands can be rationally designed and fully characterized by a number of different techniques. All the results are critically evaluated by means of a MO theoretical investigation that addresses stimulating questions about the electronic structure and the bonding in the complexes.

A preliminary account of part of this work has already been given.[5,6]

Results

Synthesis, Characterization, and Structural Analysis. It is well recognized that terminal-hydrido-metal complexes can be successfully used to synthesize polynuclear hydrido-bridged species according to the donor-acceptor scheme shown in eq 1.[7] A logical

$$L_nMH_x + M'L'_n \rightarrow L_nM(\mu\text{-}H)_xM'L'_n \qquad (1)$$

candidate for such reactions appears to be the rhodium(III) trihydride (triphos)RhH_3[8] (**1**) [triphos = $MeC(CH_2PPh_2)_3$] due to the residual nucleophilic character of the three terminal hydride ligands. Indeed, **1** reacts with unsaturated fragments formed by Rh^+, Ni^{2+}, Co^{2+}, and Fe^{2+} ions and the tripodal phosphine triphos to form stable binuclear derivatives of formulas $[(triphos)Rh(\mu\text{-}H)_3Rh(triphos)]BPh_4\cdot CH_2Cl_2$ (**2**), $[(triphos)Rh(\mu\text{-}H)_3Ni(triphos)](ClO_4)_2$ (**3**), $[(triphos)Rh(\mu\text{-}H)_3Co(triphos)](ClO_4)_2$ (**4**), and $[(triphos)Rh(\mu\text{-}H)_3Fe(etriphos)](BF_4)_2$ (**5**) [etriphos = $MeC(CH_2PEt_2)_3$] (Scheme I).

Scheme I

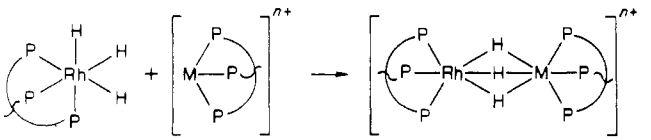

In a typical procedure, the trihydride **1** in CH_2Cl_2 is allowed to react with an equimolar amount of one of the metal fragments shown in Scheme I, in turn generated by addition of triphos to

[†] CNR.
[‡] Università di Siena.
[§] Università di Firenze.
[∥] Present address: Department of Chemistry, Northwestern University, Evanston, IL 60201.

(1) (a) Moore, D. S.; Robinson, S. D. *Chem. Soc. Rev.* **1983**, *12*, 415. (b) Hlatki, G. G.; Crabtree, R. H. *Coord. Chem. Rev.* **1985**, *65*, 1. (c) Soloveichik, G. L.; Bulydev, B. M. *Russ. Chem. Rev.* **1982**, *51*, 286. (d) Bau, R.; Carroll, W. E.; Hart, D. W.; Teller, R. G.; Koetzle, T. F. In *Transition Metal Hydrides*; Bau, R., Ed.; Advances in Chemistry 167; American Chemical Society: Washington, DC, 1978; p 73.
(2) (a) Bullock, R. M.; Casey, C. P. *Acc. Chem. Res.* **1987**, *20*, 167. (b) Lemmen, T. H.; Huffman, J. C.; Caulton, K. G. *Angew. Chem., Int. Ed. Engl.* **1986**, *25*, 262. (c) Geerts, R. L.; Huffman, J. C.; Caulton, K. G. *Inorg. Chem.* **1986**, *25*, 590. (d) Bianchini, C.; Meli, A.; Laschi, F.; Ramirez, J. A.; Zanello, P.; Vacca, A. *Inorg. Chem.* **1988**, *27*, 4429. (e) Ojima, I.; Okabe, M.; Kato, K.; Boong Kwon, H.; Horvath, I. T. *J. Am. Chem. Soc.* **1988**, *110*, 150.
(3) (a) Powell, J.; Gregg, M. R.; Sawyer, J. F. *J. Chem. Soc., Chem. Commun.* **1987**, 1029. (b) Shapley, J. R.; Richter, S. I.; Churchill, M. R.; Lashewycz, R. A. *J. Am. Chem. Soc.* **1977**, *99*, 7384.
(4) Bullock, R. M.; Samsel, E. G. *J. Am. Chem. Soc.* **1987**, *109*, 6542.
(5) (a) Bianchini, C.; Mealli, C.; Meli, A.; Sabat, M. *J. Chem. Soc., Chem. Commun.* **1986**, 777.
(6) Bianchini, C.; Meli, A.; Zanello, P. *J. Chem. Soc., Chem. Commun.* **1986**, 628.
(7) (a) Venanzi, L. M. *Coord. Chem. Rev.* **1983**, *43*, 251. (b) Albinati, A.; Lehner, H.; Venanzi, L. M. *Inorg. Chem.* **1985**, *24*, 1483. (c) Rhodes, L. F.; Huffman, J. C.; Caulton, K. G. *J. Am. Chem. Soc.* **1985**, *107*, 1759. (d) *J. Am. Chem. Soc.* **1984**, *106*, 6874.
(8) Ott, J.; Venanzi, L. M.; Ghilardi, C. A.; Midollini, S.; Orlandini, A. *J. Organomet. Chem.* **1985**, *291*, 89.

0020-1669/89/1328-2552$01.50/0

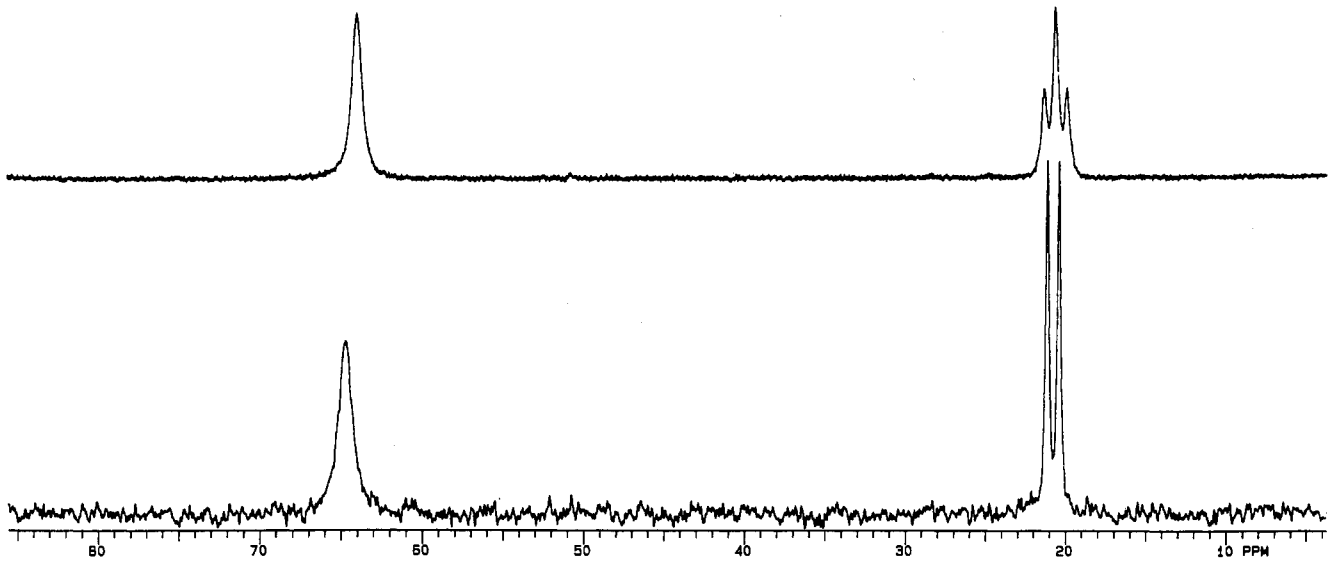

Figure 1. (a) ^{31}P NMR and (b) $^{31}P\{^1H\}$ NMR spectra of **5** (121.42 MHz, 293 K, CD_2Cl_2, 85% H_3PO_4 reference).

a solution of the appropriate, naked metal ion. Replacement of triphos with etriphos in the synthesis of **5** is necessary because of the poor ligating properties of triphos towards iron(II) cations.[9] With the exception of **5**, all of the compounds are paramagnetic with magnetic moments corresponding to one (**4**, μ_{eff} = 2.20 μ_B) or two (**3**, μ_{eff} = 3.40 μ_B) unpaired spins. A quite anomalous magnetic behavior is exhibited by **2** whose μ_{eff} value ranges over 10 preparations from 1.65 to 1.70 μ_B. No appreciable variation of the magnetic susceptibility over the temperature range 296–84 K was observed. The diffuse-reflectance spetra of the compounds are in all cases similar to the solution spectra showing the hydride complexes remain unchanged in solution. The presence of bridging hydride ligands in each member of this $(\mu\text{-H})_3$ family is indicated by broad infrared absorptions of medium intensity in the region 1610–1670 cm^{-1}.[7d] In addition, by treatment of the compounds with an excess of concentrated HCl at 60 °C in THF solution, 3 mol of H_2/mol of complex were evolved. The $^{31}P\{^1H\}$ NMR spectrum of the diamagnetic derivative **5** in CD_2Cl_2 over the temperature range 293–200 K consists of a singlet at 64.67 ppm and a doublet at 20.77 ppm (J_{PRH} = 87.5 Hz) in a 1:1 ratio (Figure 1a). The high-field signal is readily assigned to the triphos ligand bound to rhodium. The complex cation is therefore fluxional, and no coupling between triphos and etriphos is observed. The ^1H NMR spectrum in CD_2Cl_2 exhibits a double of broad doublets in the hydridic hydrogen region. Such a pattern does not vary over the temperature range 293–200 K. Irradiation at the phosphorus frequencies permits us to determine that the hydride ligands strongly couple only to the phosphorus nuclei of triphos and the rhodium atom (J_{HRh} = 27 Hz). A value of $J_{HPtrans}$ of 89.5 Hz is found, which being almost coincident with J_{PRh} makes the resonance of triphos in the ^{31}P NMR (Figure 1b) a pseudotriplet originated by two doublets overlapping at one band. Remarkably, the coupling between the trihydride bridge and the phosphorus atoms of the external tripodal ligands appears strictly dependent on the nature of the connecting metals; i.e., the magnetically inactive metal does not favor any interaction.

Because compounds **2–4** are paramagnetic, their NMR spectra do not show any resonance that may be reasonably assigned to hydrogen atoms bound to the metal. However, some valuable information on the conformational and electronic structure of the complexes is provided by ESR spectroscopy (see below).

Compounds **2–5** are quite stable in the solid state and, with the exception of **5**, remain unchanged for days in deoxygenated solutions. While the $[Rh/Co]^{2+}$ complex is practically air-stable, all of the other compounds react in solution with atmospheric oxygen. However, only in the case of the $[Rh/Rh]^+$ complex, **2**, was a well-defined product obtained. In fact **2** is slowly oxidized in DMF by atmospheric oxygen to give $[(triphos)Rh(\mu\text{-H})_3(triphos)](BPh_4)_2\cdot DMF$ (**6**), which, in turn, can be reconverted to **2** by reduction in THF with $NaC_{10}H_8$. Compound **6** is paramagnetic with a magnetic moment corresponding to one unpaired spin (μ_{eff} = 2.20 μ_B) and is air-stable both in the solid state and in solution in which it behaves as a 1:2 electrolyte. The IR spectrum contains no ν(Rh–H–Rh); however, the presence of three hydride ligands was ascertained both by decomposition of the compound with HCl and by an X-ray analysis.

The structure of **6** consists of discrete $[(triphos)Rh(\mu\text{-H})_3Rh(triphos)]^{2+}$ cations and triphenylborate anions. An ORTEP drawing of the complex dication is presented in Figure 2. Selected bond distances and angles are reported in Table I.

Table I. Selected Bond Distances (Å) and Angles (deg) for $[(triphos)Rh(\mu\text{-H})_3Rh(triphos)](BPh_4)_2\cdot DMF$

Rh1–Rh2	2.644 (1)	P2–C2	1.86 (1)
Rh1–P1	2.316 (3)	P3–C3	1.83 (1)
Rh1–P2	2.302 (3)	P4–C6	1.83 (1)
Rh1–P3	2.302 (2)	P5–C7	1.85 (1)
Rh2–P4	2.328 (2)	P6–C8	1.85 (1)
Rh2–P5	2.316 (4)	C1–C4	1.56 (1)
Rh1–P6	2.327 (3)	C2–C4	1.54 (2)
Rh1–H1B	1.81 (8)	C3–C4	1.55 (2)
Rh1–H2B	1.6 (1)	C4–C5	1.55 (2)
Rh1–H3B	1.6 (1)	C6–C9	1.57 (1)
Rh2–H1B	1.9 (1)	C7–C9	1.52 (1)
Rh2–H2B	2.1 (1)	C8–C9	1.55 (2)
Rh2–H3B	1.7 (1)	C9–C10	1.56 (2)
P1–C1	1.85 (1)		
P1–Rh1–P2	87.5 (1)	P4–Rh2–H1B	94 (3)
P1–Rh1–P3	90.8 (1)	P4–Rh2–H2B	105 (3)
P2–Rh1–P3	86.4 (1)	P4–Rh2–H3B	161 (4)
P4–Rh2–P5	89.3 (1)	P5–Rh2–H1B	166 (3)
P4–Rh2–P6	86.4 (1)	P5–Rh2–H2B	100 (3)
P5–Rh2–P6	88.5 (1)	P5–Rh2–H3B	108 (4)
H1B–Rh1–H2B	80 (5)	P6–Rh2–H1B	105 (3)
H1B–Rh1–H3B	72 (6)	P6–Rh2–H2B	166 (3)
H2B–Rh1–H3B	82 (6)	P6–Rh2–H3B	101 (4)
H1B–Rh2–H2B	66 (4)	Rh2–Rh1–P1	125.38 (6)
H1B–Rh2–H3B	66 (5)	Rh2–Rh1–P2	128.41 (7)
H2B–Rh2–H3B	66 (5)	Rh2–Rh1–P3	125.76 (8)
P1–Rh1–H1B	99 (3)	Rh1–RH2–P4	125.79 (8)
P1–Rh1–H2B	85 (3)	Rh1–Rh2–P6	128.63 (8)
P1–Rh1–H3B	165 (4)	Rh2–Rh1–H1B	46 (3)
P2–Rh1–H1B	96 (3)	Rh2–Rh1–H2B	54 (5)
P2–Rh1–H2B	171 (4)	Rh2–Rh1–H3B	40 (5)
P2–Rh1–H3B	105 (4)	Rh1–Rh2–H1B	43 (3)
P3–Rh1–H1B	170 (3)	Rh1–Rh2–H2B	37 (3)
P3–Rh1–H2B	99 (4)	Rh1–Rh2–H3B	37 (5)
P3–Rh1–H3B	98 (4)		

(9) Bianchini, C.; Dapporto, P.; Mealli, C.; Meli, A. *Inorg. Chem.* **1982**, *21*, 612.

Table II. Electrode Potentials (V) for the Redox Changes Exhibited by $[(triphos)Rh(\mu\text{-}H)_3Rh(triphos)]^{2+}$ in Different Nonaqueous Solvents

	$E^{\circ\prime}_{3+/2+}$		$E^{\circ\prime}_{2+/1+}$		$E^{\circ\prime}_{1+/0}$		$E^{\circ\prime}_{0/1-}$	
solvent	vs SCE	vs Fc^+/Fc	vs SCE	vs Fc^+/Fc	vs SCE	vs Fc^+/Fc	vs SCE	vs Fc^+/Fc
DMSO	+0.23	−0.20	−0.41	−0.84	−1.28	−1.71	−1.96	−2.39
DMF	+0.23	−0.22	−0.40	−0.85	−1.27	−1.72	−1.96	−2.41
MeCN	+0.21	−0.16	−0.46	−0.83	−1.35	−1.72	−2.04	−2.42
CH_2Cl_2	+0.35	−0.13	−0.35	−0.83	−1.34	−1.82	*a*	*a*
Me_2CO	+0.32	−0.19	−0.34	−0.85	−1.24	−1.75	*a*	*a*

[a] Obscured by the solvent discharge.

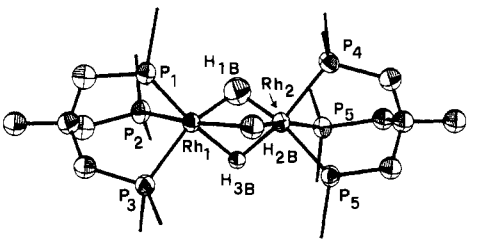

Figure 2. ORTEP drawing of the complex cation $[(triphos)Rh(\mu\text{-}H)_3Rh(triphos)]^{2+}$. For sake of clarity the phenyl substituents of triphos are omitted.

The complex dication is formed by two terminal (triphos)Rh fragments bridged by three hydride ligands. Each metal and its three phosphorus donor atoms are approximately trigonal pyramidal with P–Rh–P angles slightly less than 90°, as usually found for the rigid (triphos)Rh fragments. The two L_3Rh fragments face each other in a way to share a common pseudo-3-fold axis, but their mutual orientation is about halfway between eclipsed and staggered (the rotation of the groups about the 3-fold axis is ca. 15° from the ideal eclipsed configuration). Ultimately, if we assume that the bridging hydrogen atoms are all symmetric with respect to the two metals, the symmetry is neither D_{3h} nor D_{3d} but is approximately D_3. A most symmetrical disposition to the latter ligands was calculated by the program HYDEX[10] on the basis of the assigned Rh–H distance of 1.7 Å and their minimum repulsion energy with the rest of the molecule. Subsequent least-squares refinement shifted somewhat these ideal locations (especially for atom H2B which is at 1.6 (1) and 2.1 (1) Å from Rh1 and Rh2, respectively.) Ultimately, however, the reliability of these results is scarce. This is unfortunate because the information relative to the break of the 3-fold symmetry is quite important for the development of the subsequent theoretical arguments (vide infra). The final structural remark concerns the Rh–Rh separation of 2.644 (1) Å. This appears to be a relatively long value considering that, on the basis of the electron-counting rules, the Rh–Rh linkage is assigned a bond order of 2.5. A steric repulsion between the bulky phenyl substituents of triphos can in principle stretch the metal–metal bond, but against this argument we recall that in the analogous complex $[(triphos)Fe(\mu\text{-}H)_3Fe(triphos)]^+$ the Fe–Fe separation is as short as 2.332 (3) Å.[11]

Electrochemistry. The available data point out that it is possible to add or remove valence electrons within the $(triphos)Rh(\mu\text{-}H)_3Rh(triphos)$ framework with no consequential change of the primary geometry of the complex shown by the structure. Accordingly, we investigated in detail the electrochemistry of **2**–**5** to determine the existence of other members of the present family of bimetallic $(\mu\text{-}H)_3$ complexes. Such a study is of particular relevance in view of the scarcity of electrochemical data on metal polyhydrides in the literature.[12]

Figure 3 illustrates the cyclic voltammetric behavior of the complex cation $[Rh/Rh]^{2+}$ at a platinum electrode in deaerated

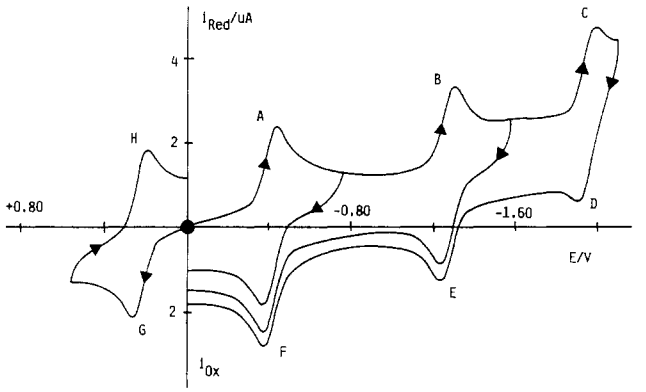

Figure 3. Cyclic voltammogram recorded on a platinum electrode on a DMSO solution containing **6** (3.5×10^{-4} mol dm^{-3}) and $[NEt_4]ClO_4$ (0.1 mol dm^{-3}). Scan rate = 0.2 V s^{-1}.

DMSO solution. Three cathodic and one anodic steps are displayed, each of which shows a directly associated response in the reverse scan. Controlled-potential coulometric tests performed in correspondence to the first cathodic process A (working potential −0.8 V) indicated the consumption of 1 mol of electrons/mol of starting dinuclear complex. Therefore, on the basis of the peak height of the remaining electron transfers, it can preliminary be deduced that $[Rh/Rh]^{2+}$ undergoes, at least in the cyclic voltammetric time scale, the five-membered redox sequence

$$[Rh/Rh]^{3+} \underset{-e^-}{\overset{+e^-}{\rightleftharpoons}} [Rh/Rh]^{2+} \underset{-e^-}{\overset{+e^-}{\rightleftharpoons}} [Rh/Rh]^{+} \underset{-e^-}{\overset{+e^-}{\rightleftharpoons}} [Rh/Rh] \underset{-e^-}{\overset{+e^-}{\rightleftharpoons}} [Rh/Rh]^-$$

The analysis of the cyclic voltammetric responses relevant to the peak system A/F and G/H with scan rates varying from 0.02 to 50 V s^{-1} reveals that the involved redox changes are attributable to simple reversible one-electron charge transfers;[13] in fact, the i_p(backward)/i_p(forward) ratio is constantly equal to 1 and the peak-to-peak value for each peak system is constantly equal to 60 mV (except that, at 20–5 V s^{-1}, values of 70–80 mV are observed, likely because of some uncompensated solution resistances). The reversibility of the electrode reactions indicates that the structural framework of the trihydride is not significantly affected by addition or removal of one electron. As far as the peak-systems B/E and C/D are concerned, the occurrence of chemical reactions following the charge transfers is hardly verifiable on the basis of the i_{pa}/i_{pc} ratio. However, the presence of associated responses in the reverse scan even at the slowest scan rate of 0.02 V s^{-1}, indicates some slow complications. This voltammetric picture holds for different nonaqueous solvents. The formal electrode potentials of all redox steps are reported in Table II. In order to directly compare the redox potentials in different solvents, the ferrocenium/ferrocene couple (Fc^+/Fc) was also used as a reference.[14]

Macroelectrolysis experiments were performed in correspondence to the first anodic process (+0.4 V) and the first cathodic process (−0.4 V) in CH_2Cl_2 solution containing $[NBu^t_4]ClO_4$ as

(10) Orpen, A. G. "HYDEX, program for locating hydrides", University Chemical Laboratories, Cambridge, England, 1977.
(11) Dapporto, P.; Midollini, S.; Sacconi, L. *Inorg. Chem.* **1975**, *14*, 1643.
(12) (a) Allison, J. D.; Walton, A. *J. Am. Chem. Soc.* **1984**, *106*, 163. (b) Mohering, G. A.; Walton, R. A. *J. Chem. Soc., Dalton Trans.* **1987**, 715. (c) Klingher, R. J.; Huffman, J. C.; Kochi, J. K. *J. Am. Chem. Soc.* **1980**, *102*, 208.
(13) Brown, E. R.; Sandifer, J. R. *Physical Methods of Chemistry. Electrochemical Methods*; Rossiter, B. W., Hamilton, J. F., Eds.; J. Wiley: New York, 1986; Vol. 2, Chapter 4.
(14) Gagnē, R. R.; Kowal, C. A.; Lisensky, G. C. *Inorg. Chem.* **1980**, *19*, 2854.

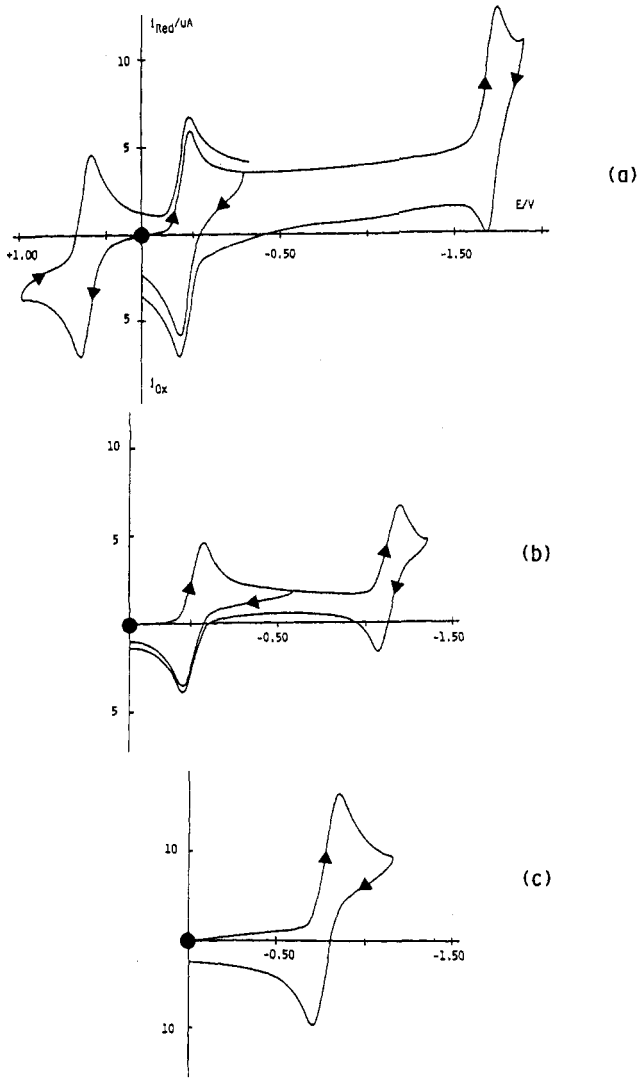

Figure 4. Cyclic voltammograms recorded at a platinum electrode: (a) MeCN solution containing **4** (3.5×10^{-4} mol dm^{-3}) and $[NEt_4]ClO_4$ (0.1 mol dm^{-3}); CH_2Cl_2 solution containing **3** (3.5×10^{-4} mol m^{-3}) and $[NBu_4]ClO_4$ (0.1 mol dm^{-3}); CH_2Cl_2 solution containing **5** (3.5×10^{-4} mol dm^{-3}) and $[NBu_4]ClO_4$ (0.1 mol dm^{-3}). Scan rate = 0.2 Vs^{-1}.

supporting electrolyte. In this way, the compounds $[(triphos)Rh(\mu\text{-}H)_3Rh(triphos)]ClO_4$ and $[(triphos)Rh(\mu\text{-}H)_3Rh(triphos)](ClO_4)_3$ could be isolated. The tetrafluoroborate derivative of the latter trication $[(triphos)Rh(\mu\text{-}H)_3Rh(triphos)](BF_4)_3$ (**7**), can be chemically synthesized by oxidation of **2** in CH_2Cl_2 with $NOBF_4$. Compound **7** is diamagnetic and is scarcely soluble in common organic solvents except DMF and nitroethane. A broad infrared absorption at 1650 cm^{-1} can be safely assigned to ν(Rh–H–Rh). The $^{31}P\{^1H\}$ NMR spectrum (DMF, 223 K) consists of a doublet at 37.09 ppm (J_{PRh} = 97.0 Hz), which becomes a doublet of quartets in the ^{31}P NMR spectrum (J_{HP} = 12 Hz). The ^1H NMR spectrum (DMF, 223 K) exhibits an unresolved multiplet at δ −12.5. These data are consistent with the presence of three magnetically equivalent hydride ligands and six equivalent phosphorus atoms.

In contrast, both the neutral and monoanionic derivatives $[Rh/Rh]^0$ and $[Rh/Rh]^-$ are stable only in the time window of cyclic voltammetry (tens of seconds). For longer times of electrolysis, the compounds decompose in correspondence to the second reduction process B (working potential −1.5 V) as shown by macroelectrolysis experiments performed in MeCN solution. In fact, cyclic voltammetry on the exhaustively two-electron-reduced solution shows ill-defined processes having no resemblance to the redox pattern of Figure 3.

Figure 4 shows the cyclic voltammograms recorded on solutions of $[Rh/Co]^{2+}$ (a), $[Rh/Ni]^{2+}$ (b), and $[Rh/Fe]^{2+}$ (c), respectively.

Table III. Electrode Potentials (V) for the Redox Changes Exhibited by $[(triphos)Rh(\mu\text{-}H)_3Co(triphos)]^{2+}$ in Different Nonaqueous Solvents

	$E^{\circ\prime}_{3+/2+}$		$E^{\circ\prime}_{2+/1+}$		$E^{\circ\prime}_{1+/0}$	
solvent	vs SCE	vs Fc^+/Fc	vs SCE	vs Fc^+/Fc	vs FCE	vs Fc^+/Fc
MeCN	+0.62	+0.24	+0.05	−0.32	−1.71	−2.09
CH_2Cl_2	+0.76	+0.27	+0.17	−0.32	−1.68	−2.12
Me_2CO	+0.72	+0.13	+0.19	−0.37	−1.51	−2.07

Table IV. Electrode Potentials (V) for the Redox Changes Exhibited by $[(triphos)Rh(\mu\text{-}H)_3Ni(triphos)]^{2+}$ and $[(triphos)Rh(\mu\text{-}H)_3Fe(etriphos)]^{2+}$ in CH_2Cl_2

	$E^{\circ\prime}_{2+/1+}$		$E^{\circ\prime}_{1+/0}$	
	vs SCE	vs Fc^+/Fc	vs SCE	vs Fc^+/Fc
$[Rh/Ni]^{2+}$	−0.05	−0.54	−1.15	−1.64
$[Rh/Fe]^{2+}$	−0.77	−1.26		

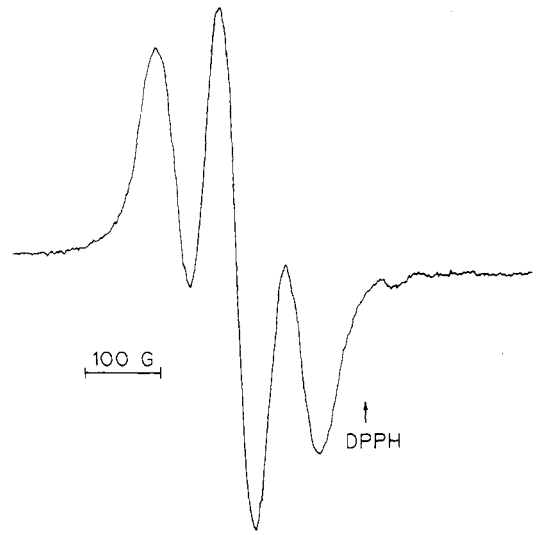

Figure 5. X-Band ESR spectrum of **10** in CH_2Cl_2 at 300 K.

The analysis of the responses coupled with controlled-potential coulometry points out the redox ability of the heterodinuclear complexes according to the sequences

$$[Rh/Co]^{3+} \underset{-e^-}{\overset{+e^-}{\rightleftharpoons}} [Rh/Co]^{2+} \underset{-e^-}{\overset{+e^-}{\rightleftharpoons}} [Rh/Co]^{+} \underset{-e^-}{\overset{+e^-}{\rightleftharpoons}} [Rh/Co]$$

$$[Rh/Ni]^{2+} \underset{-e^-}{\overset{+e^-}{\rightleftharpoons}} [Rh/Ni]^{+} \underset{-e^-}{\overset{+e^-}{\rightleftharpoons}} [Rh/Ni]^{0}$$

$$[Rh/Fe]^{2+} \underset{-e^-}{\overset{+e^-}{\rightleftharpoons}} [Rh/Fe]^{+}$$

Cyclic voltammetric tests performed at the different stages of step-by-step coulometries for the various complexes showed complete chemical reversibility only for the changes $[Rh/Co]^{3+/2+/+}$ and $[Rh/Ni]^{2+/+}$. A 20-s half-life was estimated for the $[Rh/Fe]^+$ species. Tables III and IVreport the potentials of the redox changes.

In nice agreement with the electrochemical findings, we have synthesized by chemical route the following derivatives: $[(triphos)Rh(\mu\text{-}H)_3Co(triphos)]ClO_4$ (**8**) [μ_{eff} = 3.38 μ_B; IR 1650 cm^{-1} ν(Rh–H–Co)], $[(triphos)Ru(\mu\text{-}H)_3Co(triphos)](BF_4)_3$ (**9**) [diamagnetic; IR 1650 cm$^{0-1}$ ν(Rh–H–Co)], and $[(triphos)Rh(\mu\text{-}H)_3Ni(triphos)]ClO_4$ (**10**) [μ_{ef} = 2.02 μ_B, ν(Rh–H–Ni) not detected]. The oxidations and reductions were carried out in CH_2Cl_2 solutions by using $NOBF_4$ as oxidant and $NaBH_4$ as reducing agent.

ESR Spectroscopy. Three are the compounds containing one unpaired electron, namely the dimers $[Rh/Rh]^{2+}$ (**6**), $[Rh/Co]^{2+}$ (**4**), and $[Rh/Ni]^+$ (**10**). The X-band ESR spectrum of **10** in CH_2Cl_2 at 300 K shows a pseudotriplet that can be interpreted by using a $S = {}^1/_2$ spin Hamiltonian with $\langle g \rangle$ = 2.119 (Figure 5). The hyperfine coupling constants are consistent with inter-

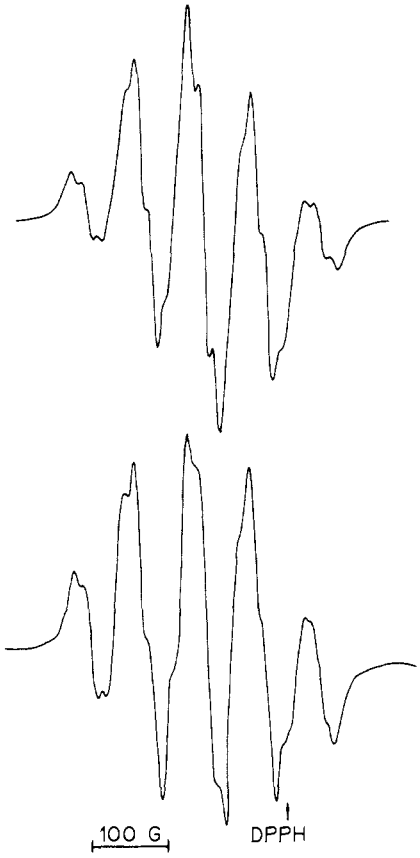

Figure 6. Experimental (a, top) and computed (b, bottom) X-band ESR spectra of **3** in CH_2Cl_2 at 300 K.

action of the unpaired electron with two almost equivalent phosphorus nuclei ($\langle A_{P1}\rangle$ = 83.0 G, $\langle A_{P2}\rangle$ = 75.0 G, $\langle \Delta H\rangle$ = 48 G). The line shape of the spectrum does not show any additional hyperfine structure. In contrast, the ESR spectra of the $[Rh/Co]^{2+}$ and $[Rh/Rh]^{2+}$ derivatives **4** and **6** in CH_2Cl_2 at 300 K consist of broad signals with no hyperfine structure with $\langle g\rangle$ values of 2.173 (ΔH_{to} = 150 G) and 2.042 (ΔH_{tot} = 60 G), respectively. No significant variation with the temperature is observed for all of these complexes; the ESR spectra of the frozen solution at 100 K invariably consist of unresolved broad signals.

As previously reported, the dimers $[Rh/Co]^{+}$ (**8**) and $[Rh/Ni]^{2+}$ (**3**) exhibit magnetic moments corresponding to two unpaired electrons. While the ESR spectrum of **8** is poorly resolved and uninformative, the spectrum of the Rh/Ni complex consists of a well-resolved pseudoquintet with $\langle g\rangle$ = 2.066 (300 K, CH_2Cl_2, $\langle \Delta H\rangle$ = 15 G), which has been simulated by considering interaction of one electron to six phosphorus nuclei (Figure 6). These are not magnetically equivalent as four different coupling constants have been used to compute the spectrum. In particular, the electron couples to two phosphorus atoms with $\langle A_P\rangle$ = 80.0 G, to two other phosphorus atoms with $\langle A_P\rangle$ = 65.0 G and to the remaining two phosphorus atoms with $\langle A_P\rangle$ = 17.0 and 15.0 G, respectively.

Finally, the monocationic $[Rh/Rh]^{+}$ derivative **2** appears ESR silent, thus indicating that the low value of the magnetic moment may be ascribed to some interaction between the two unpaired electrons.

An attempt to correlate ESR data with the electronic structure and the magnetic properties of the compounds is given in the following section.

Discussion

MO Correlations with Geometry. In light of all of the previous structural and chemical-physical data for $L_3M(\mu\text{-}H)_3ML_3$ systems, the relationships between different electron count and secondary structure (mainly the M–M separation) can be discussed in terms of MO theory. Notice that electron-counting rules predict a M≡M triple bond for 30-electron systems (d^6–d^6 metals) and that the bond order is decreased by a half unit for each additional electron.

We can start from the MO model proposed for $L_3M(\mu\text{-}H)_3ML_3$ systems by Summerville and Hoffmann,[15] which is adaptable to

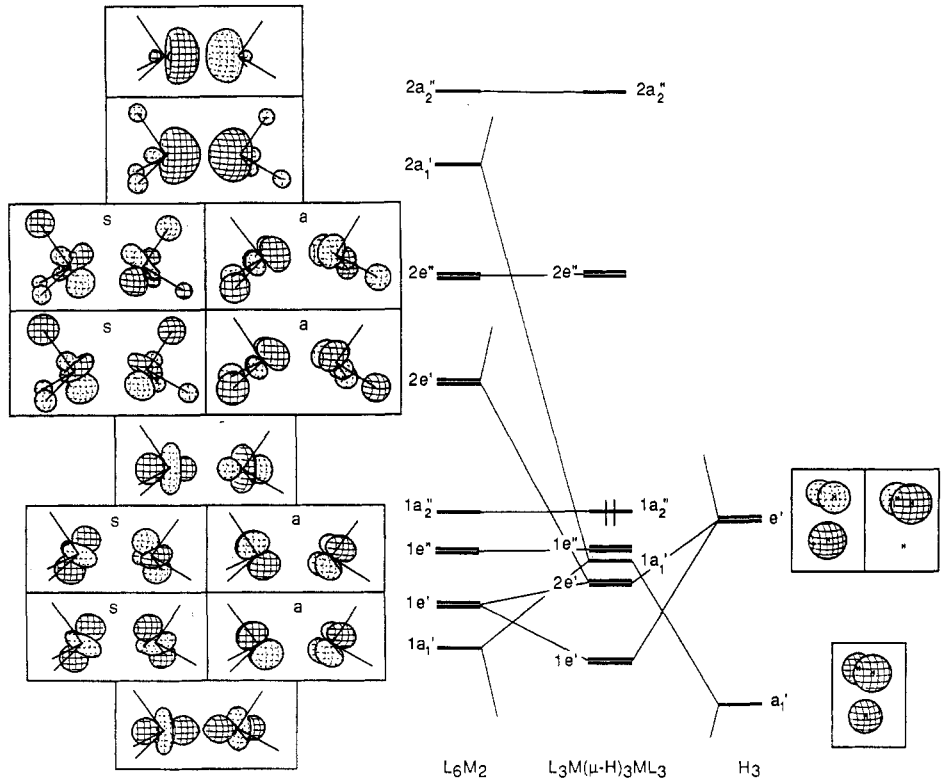

Figure 7. MO diagram for the interaction between the fragments L_6M_2 and H_3 [L = H^- and M = Rh]. The electron population of the complex (up to $1a_2''$) correspond to that of the dimer $[(triphos)Rh(\mu\text{-}H)_3Rh(triphos)]^{3+}$ with 30 valence electrons and D_{3h} symmetry. Notice that the e′ and e″ levels, at the left side of the figure, are classified as s or a, according to the symmetric or antisymmetric character with respect to the plane of the drawing.

the present compounds. In Figure 7, we report the essential features[16] of the interaction diagram between the ensemble of two L_3M fragments and the grouping of three H bridging atoms.[17] All the levels are classified according to an ideal D_{3h} symmetry. As already pointed out,[18] the energetic cost to attain other conformations, e.g. D_{3d} or D_3, is not large anyway. If each L_3M group is taken to descend from an octahedron, the fmo's at the left side are in-phase and out-of-phase combinations of the remnants of octahedral t_{2g}, e_g, and a_{1g} levels.[19]

A $L_3M{\equiv}ML_3$ compound[18] (if M = d^9, a M≡M triple bond is expected) is hardly stabilized because, with reference to the left side of Figure 7, the configuration $(2e')^4(2e'')^2$ $[=(\pi)^4(\pi^*)^2]$ would not be fully π bonding, whereas the σ orbital $2a_1'$ remains unpopulated. Thus the presence of bridging H atoms can be envisaged as a perturbation on the L_6M_2 system to cement together the two L_3M fragments. The H_3 a_1' combination (right side of Figure 7) is engaged in a three-center interaction with the metal fmo's $1a_1'$ and $2a_1'$, which are both pushed up. A similarly behavior is that of the H_3 e' level, which interacts with both the metal 1e' and 2e' levels. All the other metal levels remain unperturbed. The engagement of the L_6M_2 fmos $2a_1'$ and 2e' in bridge bonding strongly reduces their direct metal–metal-bonding character.

At this point we open a parenthesis concerning the general debate on the nature of the metal–metal bond in transition-metal clusters. Much criticism is brought up by Woolley[20] about the weakness of the EHMO method, which underestimates the contribution of d orbitals. In particular, these calculations would leave the d orbital band quite compact. Since the latter orbitals are usually filled both at the bonding and at the antibonding levels, the obvious conclusion seems that they do not participate in direct metal–metal bonding. Concerning the dimers of the type $L_3M(\mu\text{-}X)_3ML_3$ (X = H, CO), Summerville and Hoffmann[15] are not conclusive about the existence of direct M–M bonds, as the main frontier orbitals share metal–ligand- and metal–metal-bonding character. Lauher[21] classifies the metal orbitals as CVMOs (cluster valence molecular orbitals) and HLAOs (high-lying antibonding orbitals), with the latter non-d orbitals excluded from any electron assignment. However, the strong metal–metal antibonding character of HLAOs suggests that, at lower energy, the system must have bonding counterparts. In the present case, the HLAO $2a_2''$ in Figure 7 plays a precise role in the overall bonding picture of the dimer.

In a 30-electron model for $L_3M(\mu\text{-}H)_3ML_3$ (M = d^6), the MOs are populated up to $1a_2''$. Let us consider first the σ MOs. Among those derived from the "t_{2g}" group, the $\sigma(1a_1')$ and $\sigma^*(1a_2'')$ pair is populated. In principle, this seems to indicate a two-center/four-electron destabilization from which no direct metal–metal σ bond ensues. However, there is a σ^* MO ($2a_2''$) level, which lies unpopulated at high energy. Recall that the natural σ partner of the latter (the one derived from the fmo $2a_1'$) is destabilized by the interaction with the a_1' level of the bridging H_3 grouping. As a consequence, the lower filled $1a_1'$ level can be reconsidered as the potential M–M σ bonding partner of $2a_2''$. In conclusion, the metal–metal σ bond is the result of a three-orbital [$1a_1'$, $1a_2''$, $2a_2''$]/four-electron interaction rather than a more typical two-orbital/two-electron one.

What is said for σ-type interactions holds as well for π type ones; upon complex formation, $2e'/2e''$ of the unbridged L_6M_2 mojety are no longer direct π/π^* partners, since 2e' is engaged with the H_3 bridging combination e'. Ultimately, the MOs affecting direct metal–metal π interactions are 2e', 1e'', and 2e'', containing a total of eight electrons. We conclude that for a d^6–d^6 system an atypical M–M bonding network is operative. Rather than the classical filled-bonding/empty-antibonding orbital configurations $(\sigma)^2(\sigma^*)^0$ and $(\pi)^4(\pi^*)^0$, originating the M–M bonds, we have to consider the configurations $(\sigma)^2(1\sigma^*)^2(2\sigma^*)^0$ and $(\pi)^4(1\pi^*)^4(2\pi^*)^0$. Correspondingly, the M–M bond order is decreased (possibly from 3 to 1.5) if we assume that the antibonding electrons halve the strength of the bonding ones. For example, whereas the average Os≡Os triple bond is as short as 2.33 (4) Å,[22] the Os–Os distance is 2.558 Å in the $(\mu\text{-}H)_3$ dimer $[L_3Os(\mu\text{-}H)_3OsL_3]^+$ (L = PMe_2Ph),[23] a 30-electron system. Analogously, the Fe–Fe separation of 2.332 (3) Å in [(triphos)$Fe(\mu\text{-}H)_3Fe$(triphos)]$^{+}$[11] is longer than the Fe≡Fe triple bond [2.177 (3) Å] in $[(R_2R'_2C_4)Fe(\mu\text{-}CO)_3Fe(C_4R_2R'_2)]$, R = phenyl, R' = *tert*-butyl.[24] It is also longer than the ascertained Fe=Fe double bonds (ca. 2.22 Å).[25]

The presence of the 2e'' set at relatively low energy (Figure 7) is consistent with the chemical and electrochemical results, which prove that the dimers behave as electron sinks with remarkable electron-transfer properties. If any electron is added into the empty 2e'' orbitals, given their M–M π^* nature, the direct metal–metal π-bonding interaction is gradually deleted. Unfortunately, we cannot make any direct structural comparison between the electronic isomers of our series due to the already mentioned difficulties in obtaining crystals suitable for X-ray diffraction. In order to stay with isometallic species, we compare the Rh–Rh separation of the d^6–d^6 dimer $[(LL)HRh(\mu\text{-}H)_3RhH(LL)]^+$ [LL = *rac*-$Fe(\eta^5\text{-}C_5H_4PPhBut)_2$],[26] and in our d^7–d^6 dimer $[(triphos)Rh(\mu\text{-}H)_3Rh(triphos)]^{2+}$. The difference [2.594 (3) vs 2.644 (3) Å] is not large but goes in the expected direction.

At this point it is interesting to mention the prediction of Burdett and Pourian[27] about the stabilization of a polyhydrogen unit, i.e. of the existence of a bridged $(\mu\text{-}H_3)$ dimer in place of the $(\mu\text{-}H)_3$ one (I). According to these authors, the hypothetical complex

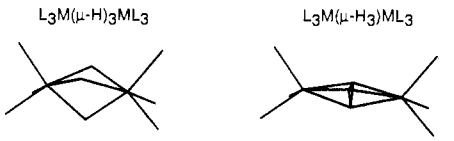

I

$(\mu\text{-}H_3)$ should be very electron rich (34 or 36 electrons) to be stable (with 2e'' and possibly a high-lying a_1' σ level totally filled).

From the geometric point of view, the formation of three H–H bonds reduces the size of the shared face of the bioctahedron and hence favors its elongation. In turn, a long M–M separation stabilizes the 2e'' level [M–M π^* in nature (Figure 7)], which becomes energetically more accessible. Eventually, four electrons in 2e'' destroy any residual M–M π bonding. According to our previous arguments, the M–M σ bonding would not completely vanish. Burdett and Pourian hypothize that also the MO descending from the fmo $2a_1'$ may be occupied (36 electrons) as it may not be too greatly destablized. Our calculation indicates that in any case the latter MO is pushed higher than $2a_2''$.

The level in question, $3a_1'$ shown in II, is mainly antibonding between the metals and the H_3 unit, and if occupied, the cementing force between L_6M_2 and the H_3 groupings would be strongly reduced. Also, the fmo a_1' of the $(\mu\text{-}H_3)$ group is quite compacted

(15) Summerville, R. H.; Hoffmann, R. *J. Am. Chem. Soc.* **1979**, *101*, 3821.
(16) The three-dimensional drawings reported throughout the paper are obtained by using the program CACAO (computer aided composition of atomic orbitals), which, as an option, allows one to separate single atomic orbital contributions. For details, see: Mealli, C.; Proserpio, D. M. To be submitted for publication.
(17) We substitute the terminal phosphine with hydrogen ligands for simplicity.
(18) For a MO treatment see: Dedieu, A.; Albright, T. A.; Hoffmann, R. *J. Am. Chem. Soc.* **1979**, *101*, 3141.
(19) Albright, T. A.; Burdett, J. K.; Whangbo, M.-H. *Orbital Interactions in Chemistry*; Wiley: New York, 1985.
(20) Woolley, R. G. *Inorg. Chem.* **1985**, *24*, 3519, 3525.
(21) Lauher, J. W. *J. Am. Chem. Soc.* **1978**, *100*, 5305.
(22) Cotton, F. A.; Walton, R. A. *Struct. Bonding* **1985**, *62*, 1.
(23) Green, M. A.; Huffman, J. L.; Caulton, K. G. *J. Organomet. Chem.* **1983**, *243*, C78.
(24) Murahashi, S.-I.; Mizoguchi, T.; Hosokawa, T.; Moritani, I.; Kai, Y.; Kohara, M.; Yasuoka, N.; Kasai, N. *J. Chem. Soc., Chem. Commun.* **1974**, 563.
(25) Cotton, F. A.; Walton, R. A. *Multiple Bonds Between Metal Atoms*; Wiley: New York, 1982; pp 296–298.
(26) Butler, I. R.; Cullen, W. R.; Tae-Jeong, K.; Einstein, F. W. B.; Jones, T. *J. Chem. Soc., Chem. Comm.* **1984**, 719.
(27) Burdett, J. K.; Pourian, M. R. *Organometallics* **1987**, *6*, 1684.

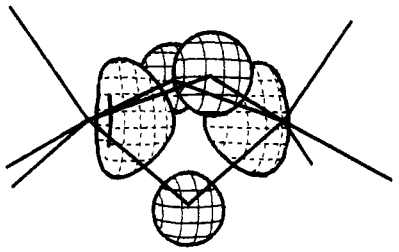

II

and overlaps better with the $1a_1'$ filled metal fmo, mainly z^2 in character. This results in a strong two-center/four-electron repulsion already transparent in the calculations of Burdett and Pourian. The latter effect raises the total energy quite a lot. Finally also the L_6M_2/H_3 e′ type interactions are much weaker because the e′ combination of the polyhydrogen (μ-H_3) unit is quite high in energy. For all these reasons, we conclude that the stabilization of a $L_3M(\mu\text{-}H_3)ML_3$ polyhydrogen compound is highly improbable, and no trace of it has been found even from electrochemical studies.

Correlations with Electrochemical and Magnetic Properties. The knowledge of the frontier MOs can be exploited to discuss, at least qualitatively, the magnetic properties of the some homometallic and heterometallic dimers. A 30-electron species such as $[(triphos)Rh(\mu\text{-}H)_3Rh(triphos)]^{3+}$ is diamagnetic, probably with a bioctahedral geometry. The latter is consistent with the NMR spectra, and it is supported by analogy with the isoelectronic $[(triphos)Fe(\mu\text{-}H)_3Fe(triphos)]^+$ complex. The HOMO/LUMO gap ($1a_2''/2e''$) is large enough to provide sufficient stability to the dimer.[28] Nonetheless one or two electrons are easily added into the 2e″ level to yield 31- and 32-electron isomers. While the odd-electron species has a magnetic moment corresponding to a single unpaired electron, the 32-electron complex shows an anomalous magnetic moment with a value much lower than that expected for two unpaired electrons (1.65 μ_B vs a theoretical spin-only value of ca. 3.0 μ_B). Moreover the magnetic moment remains constant over a wide range of temperatures. Jahn–Teller effects could be reasonably expected under the present circumstances, but before discussing them, it is opportune to remark that the degenerate e″ levels are largely centered on the metal atoms and that any contribution of the bridging hydrogen "s" orbitals is excluded by symmetry (see Figure 7). Thus, any symmetrical bending or stretching motion of the bridging hydrogen atoms within the plane orthogonal to the metal–metal vector does not split the degeneracy of the frontier levels.

A more realistic possibility to split the e″ levels by Jahn–Teller e type active vibrations is to remove the 3-fold symmetry of each terminal L_3M fragment. In the structure of **6**, each P_3Rh fragments does not have crystallographic C_3 symmetry; nonetheless, the minimum amount of the observed distortion is hardly indicative of Jahn–Teller effects. Other effects, such as spin–orbit coupling can be sufficiently large to overcome the Jahn–Teller ones. In particular, the anomalous magnetic moment of the 32-electron isomer can be explained by assuming the existence of spin–orbit coupling. A physical visualization of the latter effect is offered by Salem,[29] who suggests that each electron is allowed to enter the orbit of the second electron upon a spin inversion. Thus for some time the two electrons would have paired spins on the same MO, and such a dynamical behavior would quench part of the paramagnetism. By contrast, the lack of spin–orbit coupling can explain the different behavior of the Rh–Ni 32-electron species with respect to the Rh–Rh electronic isomer. Recall in fact that the latter complex has a magnetic moment corresponding to two unpaired electrons. Also, it presents an hyperfine ESR structure, whereas the rhodium analogue is ESR silent.

The symmetry of the heteronuclear dimers $[(triphos)Rh(\mu\text{-}H)_3Ni(triphos)]^{n+}$ (n = 1, 2) with 32 and 33 electrons can descend from C_3 to C_1 under Jahn–Teller active vibrations. One possible deformation pathway biases the plane of the three bridging H atoms toward one metal or the other (see III).

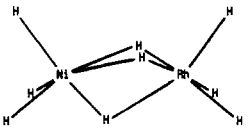

IIIa

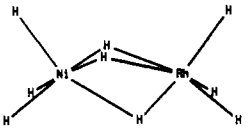

IIIb

Through the distortion and the descent of symmetry, the bridging H atom contributions may appear within the frontier 2e″ levels (Figure 7), and favor their splitting. In presence of three frontier electrons (33-electron species), the unpaired electron can be either in a MO with lobes trans to two phosphorus ligands on different metals, IV, or in an MO with lobes trans to the remaining four phosphorus ligands, V. Notice that for the undistorted

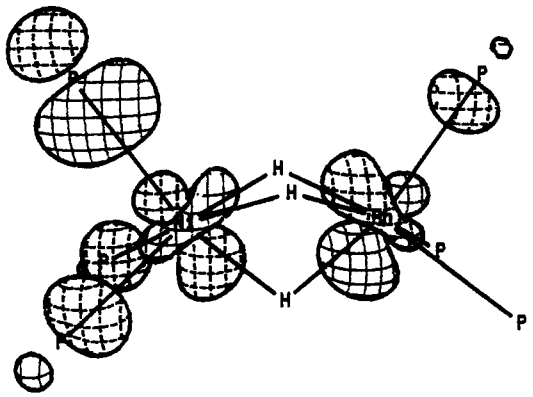

IV

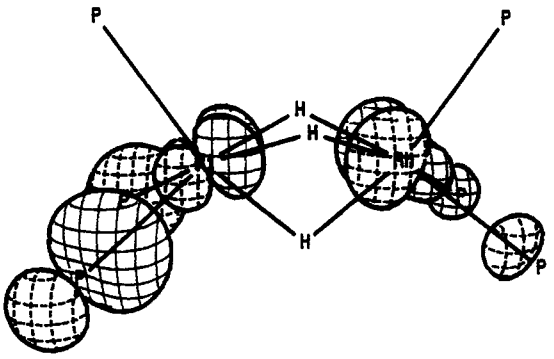

V

geometry the percentage contribution of nickel in IV and V is larger than that of rhodium (ca. 60% vs 40%). Even more dramatic is the different contribution of the phosphine ligands to the MOs in question. The phosphorous lone-pair orbitals have almost disappeared on the side of rhodium.

On a purely qualitative basis, the makeup of these MOs can be associated with the observed ESR results. For example, if the unpaired electron lies in the MO V, it spends most of its time trans to four equatorial phosphorus atoms or near to them. Consequently, the electron feels the nuclear field of the latter atoms more than the field of the other two apical P atoms. Just the opposite effect is expected if the electron is in MO IV. If the electron does not exchange between the two orbitals, an ESR triplet is expected from the former situation, whereas a quintet is expected from the latter. Actually, a pseudotriplet is observed for the $[Rh/Ni]^+$ complex (see Figure 5). This is consistent with the result calculated for model IIIa, i.e. that containing one short and two long Ni–H_b distances. In fact, a Walsh diagram shows clearly that the orbital IV destabilizes when the distortion IIIa

(28) The calculated gap is >2.0 eV for the Rh–Rh dimers, but it is about 1 eV less for the Rh–Co and the Rh–Ni species. Such a difference is consistent with the electrochemical measurements. In fact, the addition of one electron to the Rh/Co 30-electron species is more favored than that corresponding to the Rh/Rh equivalent (compare Tables II and III).

(29) Salem, L. *Electrons in Chemical Reactions: First Principles*; Wiley: New York, 1982; p 208.

is activated on account of an increased Ni–H_b antibonding.

The situation with two unpaired electrons appears more complicated. A possible rationalization is achieved only if one admits a fast exchange between the electrons that populate the two MOs IV and V. In fact, the ESR spectrum shows a pseudoquintet with pseudotriplets as superhyperfine structure. On the basis of the simulation shown in Figure 6, this spectrum may be explained by assuming that the two unpaired electrons exchange rapidly as may occur in organic biradicals when $|J| \gg |A_0|$.[30] In other words, the system behaves as it had one unpaired electron that couples to all six phosphorus atoms in the molecule. Since the equatorial ligands have a larger weight, the main structure is a quintet rather than a septuplet. Also, due to the larger contribution of the nickel and its donor phosphorus ligands in MO V, the *electron* is more sensitive to the magnetic nuclei on the nickel side. This result is experimentally confirmed by the different values of the coupling constants ($\langle A_P \rangle$ = 80.0 and 65.0 G) that are derived from the pseudoquintet structure. Finally, the superhyperfine pseudotriplet structure can be due to different couplings of the *electron* to the two axial phosphorus nuclei ($\langle A_P \rangle$ = 83.0 and 75.0 G) for the same reason as above.

Experimental Section

General Information. All reactions and manipulations were carried out under a nitrogen atmosphere. Reagent grade chemicals were used in the preparations of the complexes. The solid complexes were collected on sintered-glass frits and washed with appropriate solvents before being dried in a stream of nitrogen.

Physical Measurements. Infrared spectra were recorded with a Perkin-Elmer 475 grating spectrophotometer by using samples mulled in Nujol between KBr plates. ^1H and $^{31}P\{^1H\}$ NMR spectra were taken with a Varian CFT 20 specteometer. Peak positions are relative to tetramethysilane and phosphoric acid, respectively, with downfield values reported as positive. Conductance measurements were made with a WTW Model LBR/B conductivity bridge in ca. 10^{-3} M nitroethane solutions at 20 °C. Ultraviolet–visible spectra were recorded on a Beckman DK-2A spectrophotometer. Magnetic susceptibilities of solid samples were measured on a Faraday balance. The materials and the apparatus used for the electrochemical experiments have been described elsewhere. Unless otherwise stated, the potential values are relative to an aqueous calomel electrode (SCE). The temperature was controlled at 20 ± 0.1 °C. X-band ESR spectra were recorded with an ER 200-SRCB Bruker spectrometer operating at ν_0 = 9.78 GHz. The control of the external magnetic field was obtained with a microwave bridge ER 041 MR Bruker wavemeter. The temperature was varied and controlled with an ER 4111 VT Bruker device with an accuracy of ±1 K. In order to estimate accurate g_{iso} and g_{aniso} values over the temperature range of interest, the diphenylpicrylhydrazyl (DPPH) free radical was used as a field marker (g_{iso}(DPPH) = 2.0036). To avoid Co dipole–dipole interaction in frozen and room-temperature solutions, low concentrations were used (less than 10^{-3} M). In order to assure quantitative reproducibility, the samples were placed into calibrated quartz capillary tubes permanently positioned in the resonance cavity.

[(triphos)Rh(μ-H)$_3$Rh(triphos)]BPh$_4$·CH$_2$Cl$_2$ (2). Method A. A solution of **1** (0.36 g, 0.5 mmol) in CH_2Cl_2 (10 mL) was poured into a mixture of $[RhCl(C_2H_4)_2]_2$ (0.1 g, 0.25 mmol) and triphos (0.31 g, 0.5 mmol) in CH_2Cl_2 (15 mL). After 10 min, $NaBPh_4$ (0.17 g, 0.5 mmol) in ethanol (30 mL) was added to the resulting deep red solution. On partial evaporation of the solvent under a slow stream of nitrogen, brick red crystals precipitated in 87% yield.

Method B. A mixture of $[RhCl(C_2H_4)_2]_2$ (0.1 g, 0.25 mmol) and $AgBF_4$ (g, 0.5 mmol) in THF (30 mL) was stirred for 1 h. After AgCl was removed by filtration, solid triphos (0.31 g, 0.5 mmol) was added to the filtrate, and the resulting solution was mixed with a solution of **1** (0.36 g, 0.5 mmol) in CH_2Cl_2 (10 mL). Addition of $NaBPh_4$ (0.17 g, 0.5 mmol) in ethanol (40 mL) precipitated brick red crystals, yield 88%. Anal. Calcd for $C_{107}H_{103}BCl_2P_6Rh_2$: C, 66.00; H, 5.61; Rh, 11.05. Found: C, 65.48; H, 5.49; Rh, 10.89. Λ_M = 44 cm^2 Ω^{-1} mol^{-1}.

[(triphos)Rh(μ-H)$_3$Ni(triphos)](ClO$_4$)$_2$ (3). A solution of **1** (0.36 g, 0.5 mmol) in CH_2Cl_2 (10 mL) was added to a mixture of $Ni(ClO_4)_2$·$6H_2O$ (0.18 g, 0.5 mmol) in ethanol (30 mL) and triphos (0.31 g, 0.5 mmol) in CH_2Cl_2 (10 mL). On concentration under a slow stream of nitrogen, brownish crystals precipitated in 81% yield. Anal. Calcd for $C_{82}H_{81}Cl_2NiO_8P_6Rh$: C, 61.06; H, 5.06; Ni, 3.64; Rh, 6.38. Found: C, 61.18; H, 5.12; Ni, 3.61; Rh, 6.26. Λ_M = 88 cm^2 Ω^{-1} mol^{-1}.

[(triphos)Rh(μ-H)$_3$Co(triphos)](ClO$_4$)$_2$ (4). This green compound was obtianed in 77% yield in a manner analogous to that used to prepare **3** except for the substitution of $Co(ClO_4)_2$·$6H_2O$ for $Ni(ClO_4)_2$·$6H_2O$. Anal. Calcd for $C_{82}H_{81}CoCl_2O_8P_6Rh$: C, 61.05; H, 5.06; Co, 3.65; Rh, 6.38. Found: C, 60.98; H, 5.11; Co, 3.57; Rh, 6.31. Λ_M = 89 cm^2 Ω^{-1} mol^{-1}.

[(triphos)Rh(μ-H)$_3$Fe(etriphos)](BF$_4$)$_2$ (5). Blue crystals of **5** were prepared in 82% yield by following a procedure analogous to that reported for **3** except for substitution of a 1:1 mixture of $Fe(BF_4)_2$·$6H_2O$ and etriphos for that of $Ni(ClO_4)_2$·$6H_2O$ and triphos. Anal. Calcd for $C_{58}H_{81}B_2F_8FeP_6Rh$: C, 53.73; H, 6.29; Fe, 4.30; Rh, 7.93. Found: C, 53.54; H, 6.28; Fe, 4.38; Rh, 7.88. Λ_M = 148 cm^2 Ω^{-1} mol^{-1}.

[(triphos)Rh(μ-H)$_3$Rh(triphos)](BPh$_4$)$_2$·DMF (6). Dioxygen was bubbled through a solution of **2** (0.37 g, 0.2 mmol) and $NaBPh_4$ (0.07 g, 0.2 mmol) in DMF (5 mL) for 3 h. Alternatively, the mixture was stirred in air for 1 day. Addition of 1-butanol (30 mL) gave brick red crystals on standing; yield 86%. Anal. Calcd for $C_{133}H_{128}B_2NOP_6Rh_2$: C, 73.62; H, 5.94; Rh, 9.48. Found: C, 73.41; H, 5.87; Rh, 9.39. Λ_M = 101 cm^2 Ω^{-1} mol^{-1}.

Reaction of 6 with Sodium Naphthalenide. A solution of sodium naphthalenide, freshly prepared from naphthalene (0.07 g, 0.5 mmol) and an excess of sodium in THF (20 mL), was added dropwise to a stirred suspension of **6** (0.32 g, 0.15 mmol) in THF (20 mL). The solid dissolved to give a red solution, which was evaporated under vacuum to dryness. The excess of naphthalene was removed by sublimation at 25 °C and the residue extracted with CH_2Cl_2 (2 × 10 mL). Brick red crystals of **2** were obtained in 75% yield on addition of ethanol (30 mL) and slow concentration.

[(triphos)Rh(μ-H)$_3$Rh(triphos)](BF$_4$)$_3$ (7). A mixture of **2** (0.37 g, 0.2 mmol) and $NOBF_4$ (g, mmol) in CH_2Cl_2 (40 mL) was stirred for 10 min, during which there was a color change from red orange to bright orange. The unreacted $NOBF_4$ was removed by filtration. On addition of *n*-heptane (5 mL) to the filtrate, orange crystals precipitated, which were collected by filtration and washed with *n*-pentane; yield 65%. Anal. Calcd for $C_{82}H_{81}B_3F_{12}P_6Rh_2$: C, 57.30; H, 4.75; Rh, 11.97. Found: C, 57.08; H, 4.81; Rh, 11.76. Λ_M = 205 cm^2 Ω^{-1} mol^{-1}.

[(triphos)Rh(μ-H)$_3$Co(triphos)]Y (Y = ClO$_4$ (8), BPh$_4$ (8a)). Addition of $NaBH_4$ (0.04 g, 1 mmol) in ethanol (40 mL) to **4** (0.32 g, 0.2 mmol) in CH_2Cl_2 (20 mL) made the solution turn from green to yellow. On concentration, yellow crystals of **8** precipitated in 82% yield. Metathetical reaction of **8** with $NaBPh_4$ in CH_2Cl_2/ethanol gave **8a** in 95% yield. Anal. Calcd for $C_{82}H_{81}ClCoO_4P_6Rh$: C, 65.06; H, 5.39; Co, 3.89; Rh, 6.79. Found: C, 64.99; H, 5.33; Co, 3.81; Rh, 6.76. Λ_M = 76 cm^2 Ω^{-1} mol^{-1}. Anal. Calcd for $C_{106}H_{101}BCoP_6Rh$: C, 73.44; H, 5.87; Co, 3.39; Rh, 5.93. Found: C, 73.28; H, 5.82; Co, 3.34; Rh, 5.88. Λ_M = 46 cm^2 Ω^{-1} mol^{-1}.

[(triphos)Rh(μ-H)$_3$Co(triphos)](BF$_4$)$_3$ (9). This compound was obtained as bronzy crystals in 71% yield by the same procedure used for **7**. Anal. Calcd for $C_{82}H_{81}B_3CoF_{12}P_6Rh$: C, 58.81; H, 4.87; Co, 3.51; Rh, 6.14. Found: C, 58.88; H, 4.79; Co, 3.45; Rh, 6.03. Λ_M 204 cm^2 Ω^{-1} mol^{-1}.

[(triphos)Rh(μ-H)$_3$Ni(triphos)]Y (Y = ClO$_4$ (10), BPh$_4$ (10a)). These yellow complexes were prepared by following procedures analogous to those employed for the syntheses of **8** and **8a**. Anal. Calcd for $C_{82}H_{81}ClNiO_4P_6Rh$: C, 65.07; H, 5.39; Ni, 3.87; Rh, 6.79. Found: C, 64.93; H, 5.31; Ni, 3.84; Rh, 6.68. Λ_M = 78 cm^2 Ω^{-1} mol^{-1}. Anal. Calcd for $C_{106}H_{101}BNiP_6Rh$: C, 73.45; H, 5.87; Ni, 3.38; Rh, 5.93. Found: C, 73.32; H, 5.92; Ni, 3.31; Rh, 5.84. Λ_M = 49 cm^2 Ω^{-1} mol^{-1}.

X-ray Data Collection and Structure Determination. Crystal data for **6** are presented in Table V. A Philips PW 1100 diffractometer with Mo Kα graphite-monochromated radiation was used for experimental work. The cell constants and orientation matrix were determined by least-squares of the setting angles of 25 carefully centered reflections. Three standard reflections were measured every 120 min of X-ray exposure, and no decay with time was noted. The data were corrected for Lorentz and polarization effects. Atomic scattering factors were those tabulated by

Table V. Crystallographic Data for [(triphos)Rh(μ-H)$_3$Rh(triphos)](BPh$_4$)$_2$·DMF

$C_{133}H_{128}B_2O_1N_1P_6Rh_2$	fw = 2169.78
a = 16.868 (3) Å	space group: $P\bar{1}$ (No. 1)
b = 15.863 (6) Å	T = 22 °C
c = 14.026 (3) Å	λ = 0.710 69 Å
α, β, γ = 111.74 (3)°, 91.01 (2)°, 116.25 (3)°	ρ_{calcd} = 1.39 g cm^{-3}
V = 3051.60 Å^3	μ = 3.58 cm^{-1}
Z = 1	transmissn coeff = 0.98–0.92
$R(F_o)$ = 0.059	$R_w(F_o)$ = 0.064

(30) Wertz, J. E.; Bolton, J. R. *Electron Spin Resonance. Elementary Theory and Practical Applications*; McGraw-Hill: New York, 1975; p 250.

Cromer and Waber with anomalous dispersions corrections taken from ref 31.

The triclinic acentric space group $P1$ is evident from the analysis of a Patterson map, where one finds six, rather than three, short Rh-P vectors. The latter are consistent with a nonsymmetrical torsion of the two P_3Rh fragments about the Rh-Rh vector. This pattern has been previously found for other structures of bridged $[(triphos)M]_2$ dications and two BPh_4^- anions, e.g. $[(triphos)Co(\mu\text{-}OH)_2Co(triphos)](BPh_4)_2$,[32] which is practically isomorphous with **6**. A number of Fourier F_o and ΔF maps allowed the identification of all of the non-hydrogen atoms, including two disordered DMF solvent molecules. Least-squares refinement with the routines of the SHELX76 program package[33] was performed by the full-matrix method, initially with isotropic and then with anisotropic thermal parameters for both Rh and P atoms. The phenyl rings were treated as rigid groups of D_{6h} symmetry with C-C distances fixed at 1.395 Å and calculated hydrogen positions (C-H = 1.08 Å). Physically reasonable temperature factors were refined by assigning population parameters of 0.5 to the atoms of the DMF molecules. The bridging hydrogen ligands could not be clearly located in the final ΔF maps, although some residual electron density of ca. 1 e/Å^3 (slightly above background) appeared in the expected region. As mentioned in the description of the structure, the program HYDEX[10] was used to define good starting positions for the latter H atoms, which were then satisfactorily refined. The final R factor is 0.059 (R_w = 0.064). Refinement final coordinates of all non-hydrogen atoms (excluding rigid body atoms) and of the three bridging hydridic hydrogens are reported in the supplementary material.

Computational Details. All of the MO calculations were of the extended Hückel type[34] using a modified version of the Wolfsberg-Helmholz formula. The parameters used for Rh and P atoms are taken from ref 35. Those for the nickel atom are taken from ref 36. The H_{ii} for hydrogen is -13.6 eV, and the Slater exponent is 1.3. The (triphos)Rh fragment was most often simulated with a H_3Rh fragment with Rh-H distances of 1.7 Å and H-Rh-H angles of 90°. In cases where the terminal ligands where taken as PH_3 groups, the Rh-P distance was 2.3 Å. The metal-metal separation was fixed at 2.65 Å.

Registry No. **1**, 100333-94-6; **2**, 104119-27-9; **3**, 104119-31-5; **4**, 104119-29-1; **5**, 104138-93-4; **6**, 105736-79-6; **7**, 104103-50-6; **8**, 104119-23-5; **8a**, 120686-57-9; **9**, 104119-33-7; **10**, 104119-25-7; **10a**, 120686-58-0; $[RhCl(C_2H_4)_2]_2$, 12081-16-2; $[(triphos)Rh(\mu\text{-}H)_3Rh(triphos)]$, 120852-80-4; $[(triphos)Rh(\mu\text{-}H)_3Rh(triphos)]^-$, 120852-81-5; $[(triphos)Rh(\mu\text{-}H)_3Co(triphos)]$, 120852-82-6; $[(triphos)Rh(\mu\text{-}H)_3Fe(etriphos)]^+$, 120852-83-7; $[(triphos)Rh(\mu\text{-}H)_3Ni(triphos)]$, 120852-84-8.

Supplementary Material Available: Table SI (complete crystal data). Table SII (listings of thermal parameters), Table SIII (atomic coordinates of rigid body atoms), and Table SIV (calculated coordinates of hydrogen atoms (12 pages); a table of observed and calculated structure factors (54 pages). Ordering information is given on any current masthead page.

(31) Cromer, D. T.; Waber, J. T. *Acta Crystallogr.* **1965**, *18*, 104.
(32) Mealli, C.; Midollini, S.; Sacconi, L. *Inorg. Chem.* **1975**, *14*, 2513.
(33) Sheldrick, G. M. "SHELX76, Program for Crystal Structure Determinations", University of Cambridge, Cambridge, England, 1976.
(34) Hoffmann, R.; Lipscomb, W. N. *J. Chem. Phys.* **1962**, *36*, 2179, 3489; **1962**, *37*, 2872. Hoffmann, R. *J. Chem. Phys.* **1963**, *39*, 1397.
(35) Summerville, R. H.; Hoffmann, R. *J. Am. Chem. Soc.* **1976**, *98*, 7240.
(36) Albright, T. A.; Hofmann, P.; Hoffmann, R. *J. Am. Chem. Soc.* **1977**, *99*, 7546.

Contribution from the Departments of Chemistry, University of South Carolina, Columbia, South Carolina 29208, and Furman University, Greenville, South Carolina 29613

Isomers and Isomerizations in Heteroatomic and Substituted P_7^{3-} and Related Systems

Benjamin M. Gimarc*,† and Jane J. Ott‡

Received November 2, 1988

The ion P_7^{3-} is fluxional in solution. Baudler and co-workers have proposed a mechanism for the framework reorganization involved. Isoelectronic and isostructural but heteroatomic systems such as P_6As^{3-}, $As_3S_4^+$, and P_4S_3 are known and present the possibility of positional isomers. If activation barriers to rearrangement are comparable to those in P_7^{3-}, then these heteroatomic systems might undergo isomerization reactions. The various isomers can be conveniently related by reaction graphs derived from the proposed rearrangement mechanism. In reaction graphs vertices represent individual isomers and edges linking the vertices correspond to rearrangement processes. The reaction graph outlines the appropriate cuts through the energy surface along the overall reaction path. Relative energies or stabilities of isomers can be estimated by using the rule of topological charge stabilization. In this paper reaction graphs and relative isomer energies are presented and used to rationalize the existence of known isomers and to predict the existence of others among the binary cluster compounds A_6B, A_5B_2, and A_4B_3 related to P_7^{3-}.

Introduction

In the crystalline state, the ion P_7^{3-} has the cluster or cage-shaped structure **1**.[1]

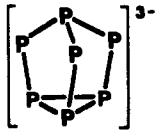

1

In solution at 80 °C the ^{31}P NMR spectrum shows that all atoms are equivalent; the ion is fluxional.[2,3] Baudler and co-workers have proposed a mechanism (eq 1) to account for the structural reorganization that takes place. This is a degenerate rearrangement or pseudorotation that restores the original structure but with a new orientation in space. They note the similarity between eq 1 and the degenerate Cope rearrangement

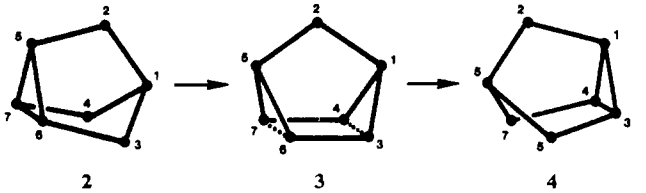

2 **3** **4** (1)

of bullvalene, $C_{10}H_{10}$.[4,5] The barrier to rearrangement is 10-12 kcal/mol. Böhm and Gleiter have studied this rearrangement with MINDO/3 calculations and rationalized the low activation barrier using qualitative MO theory.[6] X-ray studies of crystals containing

† University of South Carolina.
‡ Furman University.

(1) von Schnering, H. G.; Menge, G. *Z. Anorg. Allg. Chem.* **1981**, *481*, 33.
(2) Baudler, M.; Ternberger, H.; Faber, W.; Hahn, J. *Z. Naturforsch.* **1979**, *34B*, 1690.
(3) Baudler, M. *Angew. Chem., Int. Ed. Engl.* **1982**, *21*, 492.
(4) Schröder, G. *Angew. Chem., Int. Ed. Engl.* **1963**, *2*, 481.
(5) Doering, W. v. E.; Roth, W. R. *Angew. Chem., Int. Ed. Engl.* **1963**, *2*, 115.

0020-1669/89/1328-2560$01.50/0